ACS Catalysis

Research Article

pubs.acs.org/acscatalysis

Pd Nanoparticles on Carbon Nitride–Graphene for the Selective Electro-Oxidation of Glycerol in Alkaline Solution

Haibo Wang,[†] Larissa Thia[§,‡] Nan Li,[†] Xiaoming Ge,[§] Zhaolin Liu,[§] and Xin Wang*[,†]

[†]School of Chemical and Biomedical Engineering, Nanyang Technological University, 62 Nanyang Drive, Singapore 637459

[‡]Interdisciplinary Graduate School, Nanyang Technological University, 50 Nanyang Avenue, Block S2-B3a-01, Singapore, 639798

[§]Institute of Materials Research and Engineering, Agency for Science, Technology and Research (A*STAR), 3 Research Link, Singapore 117602

Supporting Information

ABSTRACT: A hybrid support consisting of carbon nitride and graphene (CN_x/G) is prepared by annealing polypyrrole/GO at 800 °C. Pd nanoparticles (NPs) are then loaded onto the support by a microwave–polyol method. Pd-CN_x/G is used as a catalyst for glycerol electro-oxidation in 0.5 M NaOH aqueous solution. Electrochemical characterization and product analysis by high-performance liquid chromatography show that, in comparison to Pd NPs supported on carbon black, Pd NPs on a support containing nitrogen atoms has the ability to promote selectivity toward C3 products as well as increase activity. The main factors influencing the selectivity and activity are also discussed.

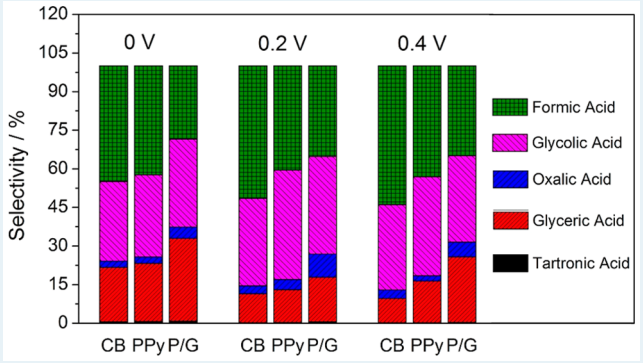

KEYWORDS: *glycerol oxidation, selectivity, carbon nitride, Pd nanoparticle, graphene*

INTRODUCTION

Recently, the growth of the biodiesel industry has greatly increased the production of glycerol.[1,2] Employing glycerol as fuel for the cogeneration of valuable chemicals and electricity has been proposed as a promising way to utilize glycerol. Although the mechanistic study of glycerol electro-oxidation in alkaline solution began 20 years ago, few investigations have been devoted to this subject, due to its complexity.[3−6] Electro-oxidation of glycerol gives rise to various products, such as glyceric acid, hydroxypyruvic acid, mesoxalic acid, tartronic acid, and other C2 or C1 products via C−C bond breaking.[7−9] The diverse range of products renders it challenging to control both activity and selectivity during the electro-oxidation process.

Several strategies have been developed to improve product selectivity during glycerol electro-oxidation. One approach is via the mediation of other molecules and adatoms. For example, with the presence of TEMPO (2,2,6,6-tetramethylpiperidine-1-oxyl) in buffer solution (pH 9.1), 1,3-dihydroxyacetone (DHA) can be selectively oxidized from glycerol.[10] Kwon et al. applied several kinds of adatoms (Bi, Sb, Pb, In and Sn) on the surface of Pt and found that glycerol was fully converted to DHA when Bi was present in the solution.[11,12] Selectivity can also be controlled by tuning the operating conditions. Kim et al. achieved a glyceric acid selectivity of 87% in the continuous-flow electrocatalytic reactor at 60 °C after 10 h.[13] The Li group obtained high selectivity toward tartronic acid, glycolic acid, and mesoxalic acid in a fuel cell when the temperature, potential, and flow rate of the cell were optimized.[14−17] In other studies, Pd alloyed with other metals was used to investigate the electro-oxidation of glycerol. Simões et al. showed that different Pd alloys produced different products.[18] Zalineeva at al. studied the electrocatalytic behavior of PdBi alloys during glycerol oxidation.[19,20] On the other hand, Marchionni et al. loaded Pd nanoparticles (NPs) on a (Ni–Zn)/C support. However, limited improvements in selectivity were observed.[21]

Herein, we demonstrated that selectivity of Pd NPs for glycerol electro-oxidation could be improved by tuning the metal–support interaction. Our previous study showed that extended polymer chains can largely change the electronic property of Au NPs and greatly enhance the selectivity to glyceric acid.[22] As such, we developed a catalyst containing Pd NPs which are supported on the surface of carbon nitride/graphene (Pd-CN_x/G) support which was annealed from polypyrrole/GO (PPy/G). The existence of nitrogen in carbon materials could enhance the interaction between metal NPs and support and thus increase its activity in reactions such as the electro-oxidation of methanol, the liquid-phase oxidation of alcohols, and oxygen reduction.[23−26] However, there has been no report on the effect of metal–nitrogen interactions in glycerol electro-oxidation. In this work, we found that the

Received: January 28, 2015
Revised: March 22, 2015
Published: April 17, 2015

DOI: 10.1021/acscatal.5b00183
ACS Catal. 2015, 5, 3174−3180

interaction between Pd NPs and nitrogen-containing carbon materials not only increased the activity but also enhanced the selectivity of C3 products during glycerol electro-oxidation. Furthermore, due to the high surface area of graphene,[27] the synthesized CN_x/G results in Pd NPs of smaller sizes. This also benefits the production of C3 products.

EXPERIMENTAL SECTION

Materials. Chemicals used in this work were purchased from Sigma-Aldrich.

Preparation of Catalysts. GO was synthesized from graphite flakes by using a modified Hummers method.[28] It includes two steps: a preoxidation step and an oxidation step. In the preoxidation step, 2 g of $K_2S_2O_8$ and 2 g of P_2O_5 were first dissolved in 8 mL of 98% H_2SO_4 at 80 °C after being stirred for 10 min. A 2 g portion of graphite flakes was then added, and the suspension was stirred for 4.5 h at 80 °C. After the suspension was cooled to room temperature, the ingredients were diluted with 300 mL of DI water and filtered through a 0.2 μm Nylon membrane. The black powder was washed with DI water three times and dried in air overnight. In the oxidation step, the preoxidized graphite flakes were added to 80 mL of 98% H_2SO_4. While the temperature was kept at 5 °C by an ice bath, $KMnO_4$ was gradually added with vigorous stirring. After $KMnO_4$ was fully dissolved, the suspension was stirred at 35 °C for 2 h. A 160 mL portion of DI water was then added with stirring while the temperature was maintained at 35 °C for 2 h. After that, 460 mL of DI water and 13 mL of 30% H_2O_2 was added in sequence with vigorous stirring. The suspension was allowed to stand overnight and then centrifuged and washed with 300 mL of 10% HCl and 300 mL of DI water in sequence. After the pH of the suspension was almost neutral, 150 mL of DI water was added. The solution was ultrasonicated for 30 min. The upper solution was collected and diluted to 200 mL to obtain a GO suspension. The final concentration was estimated as about 2 wt %.

PPy/GO was synthesized according to the literature procedure with modification.[29] First, 7.2 g of cetyltrimethylammonium bromide (CTAB) was dissolved in 80 mL of a 1 M HNO_3 solution, and then 0.1 g of a GO dispersion (10 mg mL^{-1}) was added with stirring. After the temperature reached 10 °C, 0.8 g of pyrrole was added and the mixture was stirred for 60 min. A 20 mL portion of ammonium persulfate (APS, 2.7 g, molar ratio of APS to pyrrole 1/1) was added to initiate the polymerization. After 180 min, the solid product was filtered and washed with DI water and methanol in sequence and then was vacuum-dried at 40 °C for 1 day. Wire structured PPy was synthesized under the same conditions without the addition of GO.

To prepare Pd-CN_x/G, Pd-CN_x, and Pd-CB, first PPy/GO and PPy were annealed under an Ar atmosphere at 800 °C for 2 h to obtain CN_x/G and CN_x, and then 4 mg of annealed support and 1.6 mL of K_2PdCl_4/EG (3 mg mL^{-1}) were added to 10 mL of EG. The solution was ultrasonicated for 0.5 h. After 8.4 mL of EG and 0.2 mL of 2 M NaOH/EG were added, the suspension was microwaved at medium power (300 W) for 110 s using a household microwave oven. The solution was filtered and washed with ethanol several times after it was cooled. The final product was dried at 60 °C for 1 day.

Physicochemical Characterization. The morphology was observed by using scanning electron microscopy (SEM) with a JEOL JSM6701F instrument and transmission electron microscopy (TEM) with a JEOL JEM-3010 instrument. The X-ray diffraction patterns were collected with a Bruker D2 Phaser instrument. The Pd loadings in different samples were determined by inductively coupled plasma atomic emission spectroscopy (ICP-AES) on a PerkinElmer ICP Optima 2000DV instrument after samples were dissolved in 36% HCl/69% HNO_3 (3/1 v/v); Pd loadings in Pd-CB, Pd-CN_x, and Pd-CN_x/G were 24.55%, 26.35%, and 23.93%, respectively. The X-ray photoelectron spectra (XPS) were collected with a VG ESCALAB 200i-XL instrument and calibrated by the C 1s peak (284.6 eV). The BET surface area of the catalyst was measured by nitrogen adsorption/desorption at 77 K on a Quantachrome Autosorb-6B instrument. ^{13}C Nuclear magnetic resonance (NMR) spectroscopy was carried out with Bruker Avance 300 NMR spectrometer. To concentrate the sample, 5 mL of the original solution was stirred and evaporated at 80 °C for several hours until the final volume reached around 0.4 mL. Then 1 mL of D_2O was added to dissolve most of the precipitates. A 0.7 mL sample of the mixed solution was taken for the ^{13}C NMR test.

Electrochemical Characterization. Electrochemical tests of glycerol oxidation were carried out at room temperature in a conventional three-electrode cell using a Princeton Applied Research VMP2 multichannel potentiostat. Pt coil and Hg/HgO (6 M KOH) were used as the counter and reference electrodes; a 5 mm diameter glassy-carbon electrode or carbon paper (CP, 1 × 1 cm^2, Gashub) was used as the working electrode. The glassy-carbon-based working electrode was prepared as follows: first 1 mg of the catalyst was dispersed in 1.45 mL of ethanol solution by ultrasonication for 5 min, and then 0.05 mL of 0.5 wt % Nafion solution was added and ultrasonicated for 10 min to give a black dispersion. After that, 30 μL of the dispersion was dropped on the glassy-carbon electrode and dried to reach a loading of 0.01 mg cm^{-2}. For the preparation of the CP-based working electrode, 1 mg of the catalyst was dispersed in 0.3 mL of ethanol and 0.05 mL of 0.5 wt % Nafion solution, and then the dispersion was dropped onto CP to prepare a sample with a loading of 1 mg cm^{-2}. After it was dried, the working electrode was immersed in 0.5 M NaOH + 0.5 M glycerol with stirring for 10 h to fully saturate the electrode and then washed carefully with DI water. The electrode was immersed in 20 mL of 0.5 M NaOH + 0.5 M glycerol solution during the test. Then 1 mL of the solution was collected for high-performance liquid chromatography (HPLC) analysis after the specific potential was applied on the working electrode for 2 h.

CO stripping measurements were carried out in 0.5 M $HClO_4$ by using Ag/AgCl (saturated KCl) as the reference electrode. After the potential was held at 0 V for 40 min while CO was purged into the solution, the glassy-carbon electrode was removed from the solution and immersed in fresh 0.5 M $HClO_4$ which was pretreated by purging with N_2 for 30 min. CV measurements then were collected by scanning from −0.166 to 1.2 V at a scan rate of 50 mV s^{-1}. The oxidation charge of a CO monolayer on a Pd surface is assumed to be 420 μC cm^{-2}.

Chromatographic Analysis of Products. The obtained products were analyzed by using an Alltech OA-1000 Organic Acid column for high-performance liquid chromatography (HPLC, Agilent 1260 Infinity). The eluent was sulfuric acid (4 mM). During the test, 10 μL of the sample was injected into the column and the temperature of the column was kept at 80 °C. The flow rate was 0.2 mL min^{-1}. The separated compounds were detected with both a refractive index (RID) detector and a

DOI: 10.1021/acscatal.5b00183
ACS Catal. 2015, 5, 3174−3180

UV−vis detector. The standard solutions of the various products from glycerol oxidation were prepared and analyzed under the same conditions to produce the calibration curves.

RESULTS AND DISCUSSION

CN_x/G and CN_x were synthesized from PPy/GO and wire structured PPy, respectively, by annealing them at high temperature (Figure S1 in the Supporting Information). In Figure S1a, it was observed that wire structured CN_x experienced some degree of aggregation. However, in the case of CN_x/G, CN_x is loaded on the surface of graphene, which possesses a larger surface area. This is confirmed by the calculated BET surface area (Figure S2 in the Supporting Information). In XPS spectra, the N 1s peak of CN_x/G can be deconvoluted into four peaks (Figure 1), with pyridinic N,

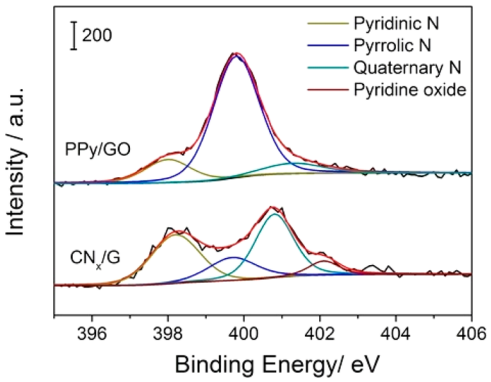

Figure 1. N 1s XPS spectra of PPy/GO and CN_x/G, obtained by annealing PPy/GO at 800 °C.

pyrrolic N, quaternary N, and pyridine oxide at 398.2, 399.7, 400.8, and 402.1 eV, respectively.[30] In comparison to the N 1s peak of PPy/GO, CN_x/G shows the obvious increment in the pyridinic N and quaternary N peaks while simultaneously showing a sharp decrement in the pyrrolic N. This demonstrates that most of the pyrrolic N in polypyrrole has been converted into pyridinic N and quaternary N after high-temperature annealing, resulting in the formation of carbon nitride materials.

Pd NPs were then loaded onto the respective supports via the microwave−polyol method. XRD patterns of Pd-CB, Pd-CN_x, and Pd-CN_x/G show the typical face-centered cubic (fcc) structure of Pd (Figure 2d). Peaks present at 40.2, 46.8, 68.2, and 82.1° can be assigned to the (111), (200), (220) and (311) facets, respectively. Pd NPs on the CN_x/G support show lower peak intensity in comparison with Pd NPs on CN_x and CB. This indicates a smaller particle size of Pd NPs on CN_x/G. From the Scherrer formula, we estimate that the mean particle sizes of Pd-CB, Pd-CN_x, and Pd-CN_x/G obtained from XRD patterns are 7.5, 7.6, and 6.9 nm, respectively.

TEM analysis was carried out to further confirm the different size distributions (Figure 2a−c). It is observed that the size of Pd NPs on CN_x/G support is smaller than those present on the CB and CN_x supports. The mean diameter of Pd NPs on CN_x/G is 4.40 nm, while it is 5.79 nm on CB and 6.30 nm on CN_x. From nitrogen adsorption−desorption isotherms (Figure S2 in the Supporting Information), the BET surface areas of CN_x, CN_x/G, and CB are calculated as 151, 168, and 194 m^2/g, respectively. Since CN_x has the smallest surface area, Pd NPs formed on its surface have the largest size. In comparison to CN_x, CN_x/G shows a larger surface area. Although its surface area is still lower than CB, the existence of nitrogen atoms might faciliate the Pd NPs on CN_x/G to exhibit the smallest size distribution.

In the TEM images (Figure 2), the aggregation of Pd NPs is observed in all these samples due to the high loading. In order to examine the extent of aggregation, we studied the Pd utilization of these catalysts. CO stripping was carried out to obtain the electrochemical active surface area (EASA) (Figure 3). CO stripping is a common way to calculate the EASA of Pd through oxidation of absorbed CO. As shown in Figure 3a−c, an obvious CO stripping peak at around 0.75 V is observed. The calculated ECSAs of Pd-CB, Pd-CN_x, and Pd-CN_x/G are 274, 258, 318 $cm^2\ mg^{-1}$, respectively. Pd NPs on a CN_x/G support show the largest EASA. The chemical surface area (CSA) is derived from the equation CSA = $6/(\rho_{Pd}\bar{D})$ (where ρ_{Pd} is 12 g/cm^3 and $\bar{D}$ is the mean diameter) (Table 1), and Pd utilization is derived from the equation Pd utilization = EASA/CSA. Pd-CN_x/G shows the smallest Pd utilization, while Pd-CN_x and Pd-CB show similarly high Pd utilizations. This means that Pd NPs on CN_x/G experienced the largest degree of aggregation, although the differences among these catalysts are small.

The electrocatalytic activity of the catalysts toward glycerol oxidation in alkaline solution was studied first using a glassy-carbon working eletrode. It was observed that Pd-CN_x and Pd-CN_x/G show higher mass-specific peak current densities in comparison to Pd-CB (Figure 4a). They also exhibited higher peak current densities normalized by ECSA (Figure S3 in the Supporting Information). When it is taken into account that Pd NPs on CN_x had the largest mean diameter while Pd supported on CNx/G had the smallest diameter, the high peak current density of both catalysts indicates that the interaction between Pd NPs and nitrogen atoms is the dominant contributing factor to the high electrocatalytic activity rather than particle size. The accelerated durability test of these catalysts in the same setup indicates that Pd NPs on CN_x/G show slightly better activity (in terms of mass-specific peak current density) throughout the test period. The improved activity and stability of Pd-CN_x/G makes it a potential catalyst for glycerol oxidation.

Catalytic activity was also examined at a loading of 1 mg cm^{-2} on a carbon-paper-based working electrode. It is observed that the current density of Pd-CN_x/G is much higher than that of Pd-CB (~1.5 times) at a potential of 0 V (Figure 5a). From this we can conclude that Pd-CN_x/G demonstrates higher activity than Pd-CB. Tests at other potentials also support this point (Figure S4 in the Supporting Information). However, when the potential is increased to 0.6 V, the current density of catalysts drops sharply (Figure 5b). This was also observed in a previous study where Pd was used as a catalyst in a direct formate fuel cell.[31] This is due to the formation of Pd oxide on the surface,[32] which drastically decreases the activity of catalysts. Interestingly, the concentration of formic acid reaches its highest value while those of other components decrease drastically when the deactivation occurs (Figure S5 in the Supporting Information). This means that glycerol is mainly oxidized to formic acid (~70%) on the surface of Pd oxide at high potentials.

The selectivity of different catalysts was studied on a glassy-carbon-based electrode (Figure 6a). When Pd-CB was used as catalyst, the concentration of formic acid was much higher than the total concentration of glycolic acid and oxalic acid (~10−20% higher). However, the amount of formic acid produced is

DOI: 10.1021/acscatal.5b00183
ACS Catal. 2015, 5, 3174−3180

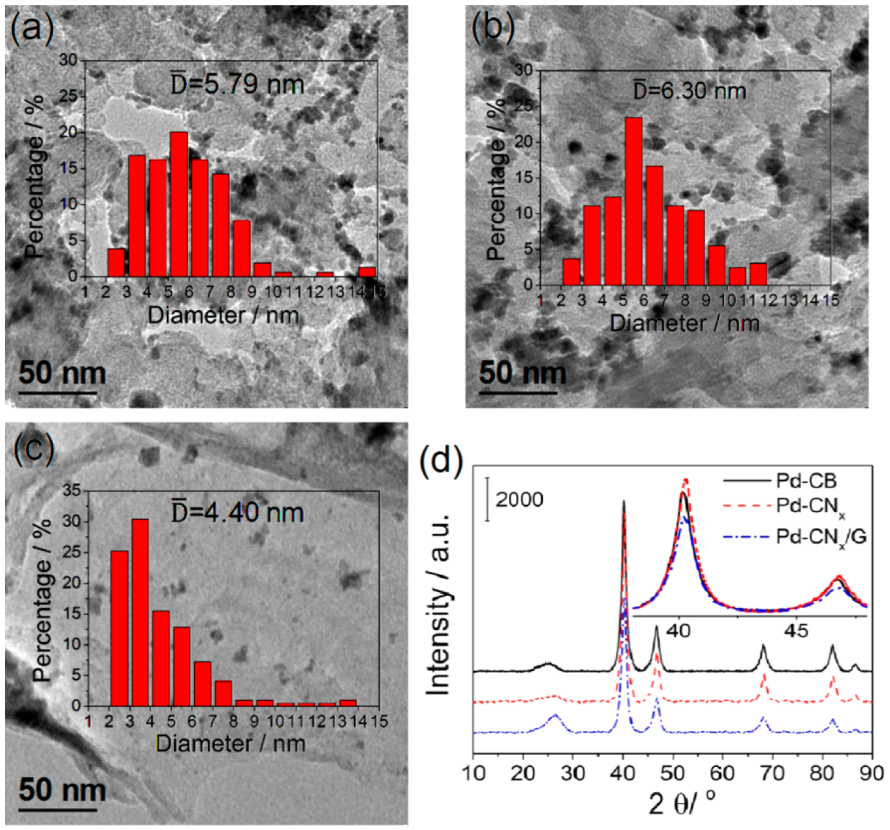

Figure 2. TEM images of (a) Pd-CB, (b) Pd-CN$_x$, and (c) Pd-CN$_x$/G. Insets give the corresponding particle size histograms. (d) X-ray diffraction (XRD) patterns of Pd-CB, Pd-CN$_x$, and Pd-CN$_x$/G.

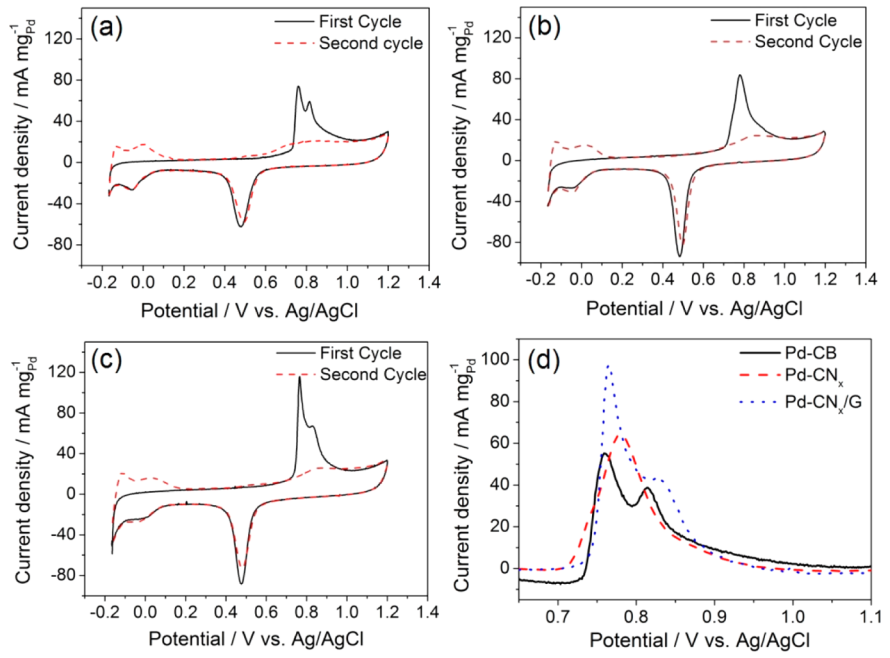

Figure 3. CO stripping voltammetry of (a) Pd-CB, (b) Pd-CN$_x$ and (c) Pd-CN$_x$/G in 0.5 M $HClO_4$ solution at a scan rate of 50 mV s^{-1}. (d) CO stripping peaks plotted for different samples. The current has been derived by subtracting the first cycle from the second cycle.

far more than the total amount of glycolic acid and oxalic acid, especially considering that some of the formic acid produced can be converted to carbonate.[21,33,34] We have also conducted carbon balance analysis on the glycerol electro-oxidation process, and the results are given in Table S1 in the Supporting Information. It can be seen that there is around 20% carbon deficiency. Since HPLC was used for the determination of various products and the relevant errors introduced during the sampling and measurement are within 3%, the observed carbon deficiency is mainly due to the formation of carbonate ion. The

DOI: 10.1021/acscatal.5b00183
ACS Catal. 2015, 5, 3174−3180

Table 1. Particle Size, ECSA, CSA, and Utilization of Catalysts

sample	particle size/ nm	ECSA/cm^2 mg_{Pd}^{-1}	CSA/cm^2 mg_{Pd}^{-1}	η_{Pd}/%
Pd-CB	5.79	283	863	32.8
Pd-CN_x	6.3	258	793	32.5
Pd-CN_x/G	4.4	318	1136	28.0

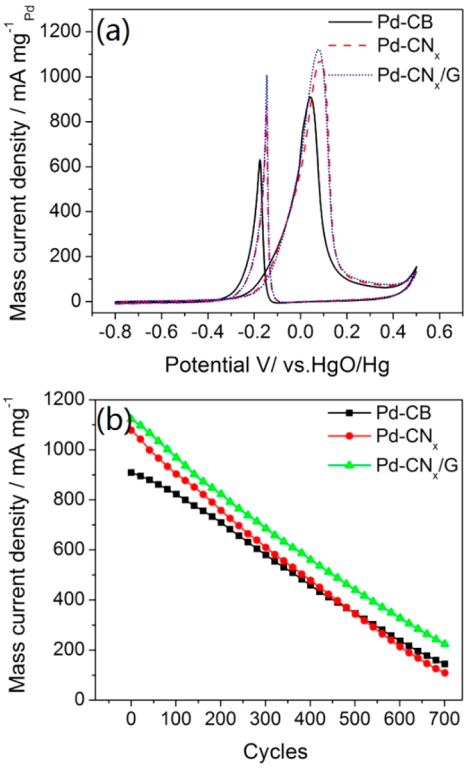

Figure 4. (a) Cyclic voltammograms (CV) and (b) accelerated durability tests of Pd-CB, Pd-CN_x, and Pd-CN_x/G in 0.5 M glycerol + 0.5 M NaOH with a scan rate of 50 mV/s. In the accelerated durability test, the potential scan was performed from −0.8 to 0.5 V and data were collected after 20 cycles.

formation of carbonate ion is confirmed by the peak at a chemical shift of 168 ppm in the ^{13}C NMR spectrum (Figure S6 in the Supporting Information).[21] Unfortunately, HPLC cannot detect the formation of carbonate or CO_2. Nevertheless, the relative ratio among all the products (i.e., selectivity) obtained will remain valid (Table S2 in the Supporting Information). In the oxidation process, it is likely that some

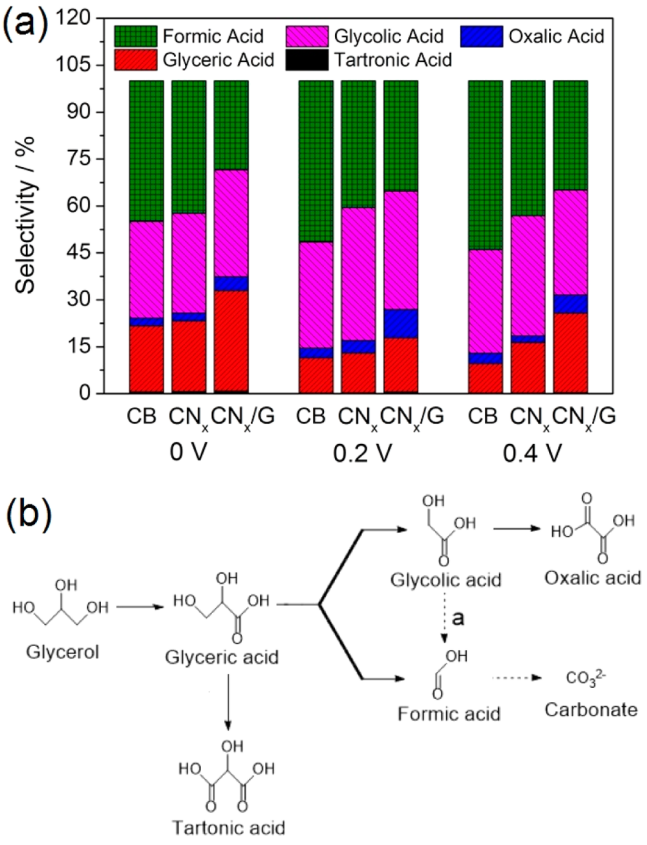

Figure 6. (a) Product selectivity of Pd NPs on different supports (CB, CN_x, CN_x/G) at various potentials. The catalyst loading is 0.1 mg cm^{-2}, and the working electrode is glassy carbon. (b) Mechanistic scheme of glycerol oxidation.

glycolic acid was oxidized into formic acid through path a (Figure 6b) on Pd-CB. However, in the case of Pd-CN_x/G, the amount of formic acid is slightly lower than the total amount of glycolic acid and oxalic acid. This means that path a is suppressed with Pd-CN_x/G. Moreover, the concentration of oxalic acid is slightly higher than that on Pd-CB, suggesting that the oxidation of glycolic acid on Pd-CN_x/G favors the path of oxalic acid.

From the product analysis, Pd-CN_x/G shows enhanced selectivity toward glyceric acid (~10−15% higher) and reduced selectivity toward formic acid (~15% lower) in comparison to Pd-CB. Although the concentration of oxalic acid also increases, the ratio between C3 products and other products in Pd-CN_x/G is still much higher than that in Pd-CB (1.8 times at 0 and

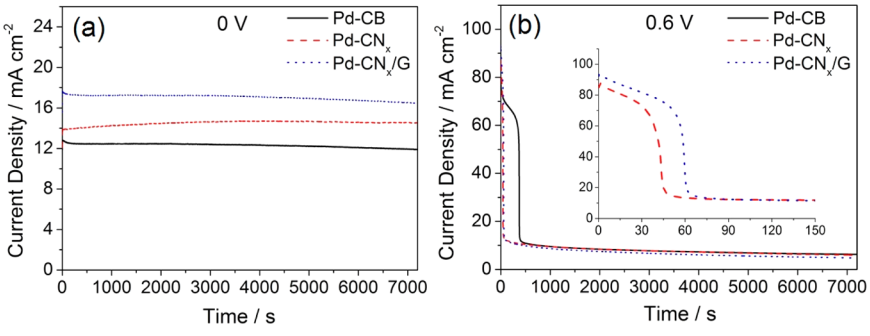

Figure 5. Chronoamperometry curves of Pd-CB, Pd-CN_x, and Pd-CN_x/G at (a) 0 V and (b) 0.6 V with a loading of 1 mg cm^{-2} on 1 cm^2 carbon paper. The inset in (b) gives the enlarged curves of Pd-CN_x and Pd-CN_x/G.

DOI: 10.1021/acscatal.5b00183
ACS Catal. 2015, 5, 3174−3180

0.2 V and 3.4 times at 0.4 V in comparison to Pd-CB). The ratio of C3 products in Pd-CN_x/G is also higher than that in Pd-CN_x (Figure 6a). This is likely due to the smaller size of Pd NPs on CN_x/G in comparison to that of the latter. Moreover, despite its larger particle size, higher selectivity toward C3 products on Pd-CN_x in comparison to that on Pd-CB was observed. This indicates that the interaction between Pd NPs and nitrogen atoms plays a more important role in the improvement of selectivity. As shown in a previous study, the interaction between metal NPs and adatom-doped carbon support as well as the metal particle size can tailor the electronic properties of metal nanoparticles.[35,36] This may weaken the adsorption ability of metal NPs toward C3 products, especially glyceric acid. Considering the competitive adsorption among C3 products and other species, weaker adsorption means the oxidation of C3 products is not preferred in comparison with other species and more C3 products are obtained. Therefore, these two factors enable Pd-CN_x/G to be more selective toward C3 products in comparison to the other two catalysts.

CONCLUSIONS

Pd NPs supported on CN_x/G have been developed as electrocatalysts for glycerol oxidation. The larger surface area of CN_x/G in comparison to CN_x results in smaller Pd nanoparticles being loaded on its surface. Due to the smaller particle size and nitrogen interaction with Pd NPs, Pd-CN_x/G shows better activity and higher selectivity toward C3 product. Product analysis shows that part of the glycolic acid is oxidized into formic acid when Pd-CB is used as the catalyst. However, this path is likely to be suppressed when Pd-CN_x/G is used as the catalyst. This causes a decrease in the formation of formic acid in Pd-CN_x/G. In addition, in comparison to Pd-CN_x which has a larger particle size, the smaller size of Pd NPs on CN_x/G gives improved selectivity toward C3 products.

ASSOCIATED CONTENT

Supporting Information

The following file is available free of charge on the ACS Publications website at DOI: 10.1021/acscatal.5b00183.

SEM images of CN_x and CN_x/G, nitrogen adsorption−desorption isotherms of different supports, cyclic voltammograms of catalysts normalized by ECSA, chronoamperometry curves at 0.2 and 0.4 V, concentration of products of catalysts produced at different potentials, carbon deficiency of the glycerol oxidation over different catalysts at selected potentials, ratios of different products assuming all other carbons are oxidized into carbonate ion and catalysts with different loading have the same carbon deficiency, and ^{13}C NMR spectra of solution using Pd-CB as catalyst at a potential of 0.2 V and loading of 1 mg cm^{-2} (PDF)

AUTHOR INFORMATION

Corresponding Author

*X.W.: e-mail, WangXin@ntu.edu.sg; tel, (65) 6316 8866; fax, (65) 6794 7553.

Notes

The authors declare no competing financial interest.

ACKNOWLEDGMENTS

This project was funded by the National Research Foundation (NRF), Prime Minister's Office, Singapore, under its Campus for Research Excellence and Technological Enterprise (CREATE) program. We also acknowledge financial support from the academic research fund AcRF tier 1 (M4011020 RG8/12 and M4011253 RG 7/14) from the Ministry of Education, Singapore.

REFERENCES

(1) Bianchini, C.; Shen, P. K. *Chem. Rev.* **2009**, *109*, 4183−4206.
(2) Yu, E. H.; Krewer, U.; Scott, K. *Energies* **2010**, *3*, 1499−1528.
(3) Avramov-Ivić, M. L.; Leger, J. M.; Lamy, C.; Jović, V. D.; Petrović, S. D. *J. Electroanal. Chem. Interfacial Electrochem.* **1991**, *308*, 309−317.
(4) Avramov-Ivic, M.; Léger, J. M.; Beden, B.; Hahn, F.; Lamy, C. *J. Electroanal. Chem.* **1993**, *351*, 285−297.
(5) Roquet, L.; Belgsir, E. M.; Lbger, J. M.; Lamy, C. *Electrochim. Acta* **1994**, *39*, 2387−2394.
(6) Schell, M.; Xu, Y.; Zdraveski, Z. *J. Phys. Chem.* **1996**, *100*, 18962−18969.
(7) Bambagioni, V.; Bianchini, C.; Marchionni, A.; Filippi, J.; Vizza, F.; Teddy, J.; Serp, P.; Zhiani, M. *J. Power Sources* **2009**, *190*, 241−251.
(8) Kwon, Y.; Schouten, K. J. P.; Koper, M. T. M. *ChemCatChem* **2011**, *3*, 1176−1185.
(9) Qi, J.; Xin, L.; Chadderdon, D. J.; Qiu, Y.; Jiang, Y.; Benipal, N.; Liang, C.; Li, W. *Appl. Catal., B* **2014**, *154−155*, 360−368.
(10) Ciriminna, R.; Palmisano, G.; Pina, C. D.; Rossi, M.; Pagliaro, M. *Tetrahedron Lett.* **2006**, *47*, 6993−6995.
(11) Kwon, Y.; Birdja, Y.; Spanos, I.; Rodriguez, P.; Koper, M. T. M. *ACS Catal.* **2012**, *2*, 759−764.
(12) Kwon, Y.; Hersbach, T. J. P.; Koper, M. T. M. *Top. Catal.* **2014**, *57*, 1272−1276.
(13) Kim, H. J.; Lee, J.; Green, S. K.; Huber, G. W.; Kim, W. B. *ChemSusChem* **2014**, *7*, 1051−1054.
(14) Xin, L.; Zhang, Z.; Wang, Z.; Li, W. *ChemCatChem* **2012**, *4*, 1105−1114.
(15) Zhang, Z.; Xin, L.; Li, W. *Appl. Catal., B* **2012**, *119−120*, 40−48.
(16) Zhang, Z.; Xin, L.; Qi, J.; Wang, Z.; Li, W. *Green Chem.* **2012**, *14*, 2150−2152.
(17) Zhang, Z.; Xin, L.; Qi, J.; Chadderdon, D. J.; Sun, K.; Warsko, K. M.; Li, W. *Appl. Catal., B* **2014**, *147*, 871−878.
(18) Simões, M.; Baranton, S.; Coutanceau, C. *Appl. Catal., B* **2010**, *93*, 354−362.
(19) Coutanceau, C.; Zalineeva, A.; Baranton, S.; Simoes, M. *Int. J. Hydrogen Energy* **2014**, *39*, 15877−15886.
(20) Zalineeva, A.; Serov, A.; Padilla, M.; Martinez, U.; Artyushkova, K.; Baranton, S.; Coutanceau, C.; Atanassov, P. B. *J. Am. Chem. Soc.* **2014**, *136*, 3937−3945.
(21) Marchionni, A.; Bevilacqua, M.; Bianchini, C.; Chen, Y. X.; Filippi, J.; Fornasiero, P.; Lavacchi, A.; Miller, H.; Wang, L.; Vizza, F. *ChemSusChem* **2013**, *6*, 518−528.
(22) Wang, H.; Thia, L.; Li, N.; Ge, X.; Liu, Z.; Wang, X. *Appl. Catal., B* **2015**, *166−167*, 25−31.
(23) Ma, Y.; Jiang, S.; Jian, G.; Tao, H.; Yu, L.; Wang, X.; Wang, X.; Zhu, J.; Hu, Z.; Chen, Y. *Energy Environ. Sci.* **2009**, *2*, 224−229.
(24) Imran Jafri, R.; Rajalakshmi, N.; Ramaprabhu, S. *J. Mater. Chem.* **2010**, *20*, 7114−7117.
(25) Wang, H.; Maiyalagan, T.; Wang, X. *ACS Catal.* **2012**, *2*, 781−794.
(26) Chan-Thaw, C. E.; Villa, A.; Veith, G. M.; Kailasam, K.; Adamczyk, L. A.; Unocic, R. R.; Prati, L.; Thomas, A. *Chem. - Asian J.* **2012**, *7*, 387−393.
(27) Stoller, M. D.; Park, S.; Zhu, Y.; An, J.; Ruoff, R. S. *Nano Lett.* **2008**, *8*, 3498−3502.
(28) Kovtyukhova, N. I.; Ollivier, P. J.; Martin, B. R.; Mallouk, T. E.; Chizhik, S. A.; Buzaneva, E. V.; Gorchinskiy, A. D. *Chem. Mater.* **1999**, *11*, 771−778.

DOI: 10.1021/acscatal.5b00183
ACS Catal. 2015, 5, 3174−3180

(29) Zhang, L. L.; Zhao, S.; Tian, X. N.; Zhao, X. S. *Langmuir* **2010**, *26*, 17624−17628.
(30) Xin, L.; Zhang, Z.; Wang, Z.; Li, W. *ChemCatChem* **2012**, *4*, 1105−1114.
(31) Bartrom, A. M.; Haan, J. L. *J. Power Sources* **2012**, *214*, 68−74.
(32) Wang, Y.; Wang, X.; Li, C. *Appl. Catal., B* **2010**, *99*, 229−234.
(33) Bambagioni, V.; Bevilacqua, M.; Bianchini, C.; Filippi, J.; Marchionni, A.; Vizza, F.; Wang, L. Q.; Shen, P. K. *Fuel Cells* **2010**, *10*, 582−590.
(34) Lin, J.; Ren, J.; Tian, N.; Zhou, Z.; Sun, S. *J. Electroanal. Chem.* **2013**, *688*, 165−171.
(35) Holme, T.; Zhou, Y.; Pasquarelli, R.; O'Hayre, R. *Phys. Chem. Chem. Phys.* **2010**, *12*, 9461−9468.
(36) van Bokhoven, J. A.; Miller, J. T. *J. Phys. Chem. C* **2007**, *111*, 9245−9249.

DOI: 10.1021/acscatal.5b00183
ACS Catal. 2015, 5, 3174−3180